

FOURTH EUROPEAN ROTORCRAFT AND POWERED LIFT AIRCRAFT FORUM

Paper No. 29

HELICOPTER SIMULATION IN ATMOSPHERIC TURBULENCE

H.J. Dahl

A.J. Faulkner

MESSERSCHMITT-BÖLKOW-BLOHM GMBH

Munich, Germany

September 13 ÷ 15, 1978

STRESA - ITALY

Associazione Italiana di Aeronautica ed Astronautica
Associazione Industrie Aerospaziali

HELICOPTER SIMULATION IN ATMOSPHERIC TURBULENCE

H.-J. Dahl, A.J. Faulkner
Messerschmitt-Bölkow-Blohm GmbH
Munich, Germany
P.O. Box 801140

Summary

This paper reviews the topic of helicopter flight in wind turbulence, a topic of primary importance since it is a leading factor in pilot work load, passenger comfort and structural loadings. Whilst much has been done in the areas of turbulence and vehicle modelling for fixed wing aircraft, this is not always applicable to rotary wing aircraft since different flight regimes and principles (low speed, rotating aerofoil) require specialised models.

Part of this paper is devoted to the integration of wind gust models to helicopter simulations, highlighting their limitations and particular helicopter requirements. The options for the helicopter model are discussed, ranging from linearised to individual integrated blade response models, and exemplified with test simulation results, with the inclusion of a pilot model in the closed control loop.

Results for a helicopter flying through a 2-dimensional turbulence field are presented, with particular attention to the influence of flapping stiffness.

Notation

a_β	[m]	Equivalent flapping hinge offset (zero spring)
A_q	[mm ² s]	Integral squared error
D_β, D_α	[deg]	Longitudinal and lateral cyclic
K_p	[-]	Pilot transfer function gain
L_u, L_w	[m]	Horizontal and vertical characteristic wave length
n	[-]	Load factor
P, Q, R	[deg/s]	Helicopter roll, pitch, and yaw rates
r	[m]	Rotor radial position

R	[m]	Rotor radius
s	[-]	Laplace operator
S	[m ²]	Blade elemental area
t	[s]	Time
Δt	[s]	Sampling interval
T	[N]	Rotor thrust
T _L	[s]	Pilot lead time
T _N	[s]	Pilot lag time
U _m	[m/s]	Mean wind speed
\bar{U}_m	[m/s]	Mean wind speed at 20 m datum
U _w , W _w	[m/s]	Wind horizontal and vertical components
v	[m/s]	Relative wind speed
V _x , V _y , V _z	[m/s]	Helicopter longitudinal, lateral and vertical velocities
x	[m]	Distance across rotor disc
Y _p (s)	[-]	Pilot transfer function
β ₁ , β ₂ , β ₃ , β ₄	[deg]	Blade flap angle (4 blades)
ζ	[-]	Damping ratio
η _x , η _y	[mm]	Longitudinal and lateral cyclic at top of pilot's stick
θ, φ, ψ	[deg]	Helicopter pitch, roll, and yaw angles
σ	[-]	Standard deviation
σ _u , σ _w	[m/s]	Gust turbulence intensities
τ	[s]	Pilot's pure time delay
Φ (Ω)	[(m ² /s ²)/(rad/m)]	Gust power spectrum
ψ	[deg]	Rotor blade station
ω	[rad/s]	Frequency
Ω	[rad/s]	Rotor rotational speed
Ω	[rad/m]	Spatial frequency

1. Introduction

The modern helicopter is no longer a novelty, restricted simply to tasks where its hovering capability is mandatory. It is expected to, and does, compete on a commercial basis with other forms of transport where it has shown a greater reliability in achieving its task. For example, nearly all the lighthouses and lightships around the British coast-line are now relieved by helicopters because they have demonstrated a higher mission reliability in "completing-on-time" than the former relief boats, which were often up to seven days late. Operating to and from landing pads with restricted access, some built on top of the lantern (Figure 1), the helicopter performs in all-year-round weather conditions, in wind speeds up to 55 kt, with a reported "completion-on-time" success rate of better than 95%. For ship operations the pilot may have to cope with a 4 m heaving deck in addition to a 30 kt wind. In another example, helicopters are based on off-shore oil platforms in the North Sea to provide daily routine inter-rig transport services and also to be in immediate readiness for accident casualties.

It can be seen from these few examples that one of the commercial attractions of the modern helicopter is its ability to operate reliably in extreme weather conditions, particularly in turbulent atmospheres. Consequently, it is essential to be able to predict the gust performance during the theoretical design stage and to seek rotor improvements to simplify the task of piloting.

In this paper, the modelling and simulation aspects of the design studies are discussed, presenting some simulation results by way of illustration.

2. Simulation Modelling Elements

The simulation of a helicopter flying through a turbulent atmosphere can be divided into its constituent modelling elements as shown in Figure 2. The first task is to establish adequate representation of the atmosphere in terms of mean wind speeds and turbulence levels, with associated probability factors. This is fundamentally a meteorological activity, but it is the responsibility of the aeronautical engineer to interpret the data to suit the particular requirements of the helicopter, such as a speed range from 200 km/hr down to hover, and an altitude range from several thousand metres to zero, covering flight states in the proximity of ground obstacles. At the moment, however, it is not possible to construct wind models to cover all these requirements.

The second task is to select the helicopter model most appropriate to the investigation; to determine whether details of the blade motion are required or only the global response. Where flight performance is being investigated, and no automatic stabilization exists, it may also be necessary to include a representation of the pilot in the form of an additional dynamic element. A number of "standard pilots" are available for this element of the simulation in the form of transfer functions. Finally, some criteria are required in order to compare aircraft qualities and assess pilot work load.

2.1 Wind Modelling

Wind models fall broadly into two main categories, (Figure 3):

- a discrete, single event gust
- continuous stochastic disturbances

The discrete gust, typically a step, ramp, sine² or (1-cosine) function, is of interest during preliminary comparison of aircraft configurations, for calculating flight loads, and in numerical derivative calculations. Furthermore, in the case of the sine² or (1-cosine) function, the duration of the gust can be varied to investigate any resonance modes of the aircraft which may be excited during flight through turbulence. The continuous stochastic model, on the other hand, attempts to construct a random signal which, over a period of time, contains the amplitudes and frequency characteristics typical of atmospheric conditions.

A considerable amount has been written on the subject of wind modelling and both the discrete and stochastic types form part of routine calculations in aircraft design, as defined in aircraft specifications such as MIL-F-8785B [1] and ARB 417 [2]. Since both types of model are described in terms of the probability of reaching a specific turbulence level, so compatible discrete and stochastic models can be derived for the same intensity of air turbulence. Normally the data is categorised in terms of light, medium or severe turbulence with a corresponding probability of the gust intensity level being exceeded at any given time. Consequently, design studies can be tailored to take into account accumulative loading conditions which might affect the fatigue life of the airframe.

Much of the wind turbulence data has been collected using instrumented towers and, to a lesser extent owing to economical reasons, from flight recordings. The wide variety of collection methods and subsequent simulation applications has necessitated a common reduction method for raw data, the frozen field concept. This hypothesis, attributed to Taylor, assumes that the random turbulence pattern is frozen in space, so that, in the case of tower-based measurements, the fixed pattern is convected past the instrumentation at the mean wind speed, thus producing fluctuations in the recorded wind speed. Implicit in this model is the change of the turbulence pattern, as energy transfers take place, occurring at a much slower rate than the progress past the tower. This rather simplified view of the atmosphere, however, has been found to produce adequate results with the exception of interference effects occurring in the proximity of buildings.

The spatially frozen gust pattern is then analysed for frequency content, frequency being measured in terms of cycles per metre, and the results presented in the form of a power spectrum. Two power spectrum forms are often quoted, the von Kármán and the Dryden [1]. Since the difference between them is basically a small variation in the high frequency content [3], the Dryden model is most frequently used owing to its greater simplicity of implementation.

In both cases, however, a power spectrum, characterised by an intensity parameter σ and a wave length L to determine the high frequency cut-off point, is given for the three directional components. The intensity parameter, or standard deviation, is not only dependent on the turbulence intensity category (moderate, severe etc.) but is also a function of the height above the ground, as exemplified in Figure 4, and ground texture. The reduction in σ at low altitudes is a result of the earth's boundary layer. Thus the Dryden model specifies the frequency content of typical turbulent conditions. For a simulation model it is necessary to construct a suitable signal with identical properties.

The turbulence model for the simulation usually consists of passing a random signal, in the case of a digital simulation the output from a random number generator, with Gaussian properties, through a first order lag function,

$$G_F(s) = \frac{A}{1 + B \cdot s} \quad (1)$$

adjusting both the filter gain and time constant to produce a power spectrum match with the Dryden model. There is, however some criticism that the Gaussian source provides too regular a turbulence with insufficient large gusts and patchiness for aircraft simulators. Work is currently in progress to produce more realistic non-Gaussian models [5]. Since the Dryden model describes the turbulence in terms of spatial coordinates, a transformation to temporal coordinates is necessary for the purpose of simulation. This is achieved using the frozen field principle, considering the relative motion between the aircraft and turbulence field

$$v = U_m + V \quad (2)$$

where U_m [m/s] is the mean wind speed and V [m/s] the helicopter ground speed. For helicopter simulation, as apposed to fixed wing aircraft, it is important to include the mean wind speed in the transformation since this term, although insignificant during cruise, becomes dominant at low speed and hover. Using the relative speed v therefore, the transformation to temporal coordinates is simply,

$$\omega = \Omega \cdot v \quad (3)$$

Deriving the turbulence from a sampling process, for example a random number generator, it is important to compensate for the fact that the spectrum is dependent on the sampling frequency as shown in [4]; the compensation taking the form of a gain adjustment factor in the filter. For example, the Dryden model for the horizontal gust component as given in [1] is,

$$\Phi_u(\Omega) = \sigma_u^2 \cdot \frac{2L_u}{\pi} \cdot \frac{1}{1 + (L_u \cdot \Omega)^2} \quad (4)$$

the turbulence simulation model would be a random Gaussian signal filtered through a first order lag,

$$F_u(s) = \sqrt{\frac{2 \cdot \sigma_u^2}{a^2 \cdot \Delta t} \cdot \frac{L_u}{v}} \cdot \frac{1}{1 + \frac{L_u}{v} \cdot s} \quad (5)$$

with the sampling frequency Δt and the factor "a" to adjust the standard deviation of the noise source [4].

2.2 Helicopter Models

The selection of helicopter model depends on the assumptions made and method of solution of the equations of motion. Since the helicopter response is almost always dominated by the main rotor influence, the various models are often described by their treatment of the rotor system (see Figure 5).

The simplest method of analysis is to linearise the rotor and 6-degree-of-freedom rigid body equations into lumped rotor and body derivatives. With this type of model the dynamic motions of the blades are neglected; rotor responses to disturbances or control inputs being assumed to occur instantaneously.

The derivative model, however, only describes the helicopter motions in response to small changes away from the trimmed flight condition, so care must be exercised during the simulation to ensure that the linear region is not exceeded. Because the linearised equations are relatively simple to solve, computation times are short, making the model very attractive for broad parametric studies. It should be remembered that, in order to produce the derivatives, a separate computer program is required which would normally trim the aircraft and calculate derivatives using a fully non-linear rotor analysis. A limitation of the model is that only gusts which encompass the whole helicopter simultaneously can be investigated and in some cases, as will be shown in the examples, this assumption becomes unrealistic.

The first stage of improvement that can be made over the derivative model is to retain the non-linearities, re-trimming the helicopter for each simulation time step. The assumption of quasi-steady blade dynamics is still retained but full non-linear aerodynamics and blade element theory can be included as in classical rotor aerodynamic performance programs.

This "quasi-stationary" model has the added advantage that gust response during flight states other than steady trim can be investigated. Since a non-linear trim calculation is performed for every simulation time step, as opposed to simply once at the beginning of the derivative simulation, computation times are correspondingly longer for this model.

The next stage of refinement is to combine individual blade dynamic motion with the 6-degree-of-freedom rigid body, as illustrated in Figure 6. In this particular case, only the rotor blade flapping motion is considered but, in principle, blade lag and torsion can be included in what is basically an air resonance and blade transient model.

With this model, it is possible to investigate individual blade gust loads, stability and interaction with each other. Since blade element theory is applied to all blades, a variation in wind speed across the rotor can also be accommodated. Although the model requires a separate calculation for each individual blade, this does not necessarily mean that it requires a greater computational time than the quasi-stationary method. Under certain manoeuvre conditions, where a small integration time step is needed for reasons of flight mechanics, the individual blade method can, in fact, result in a net saving of computer time.

2.3 Integration of Wind and Helicopter Models

Computer programs were developed at MBB for each of the three helicopter models described above. In each case, the facility was included for providing both a discrete gust and stochastic turbulence over the total rotor system. Furthermore, in the case of the individual blade model, the opportunity was taken to include as an alternative, a gust field, so that the effect of gradual rotor penetration through turbulence could be investigated.

The helicopter side view shown in Figure 7 illustrates how the gust field was included in the simulation. In this particular example, the helicopter is hovering with a head wind of 5 m/s so that it takes about 2,5 seconds for a gust to pass from the leading edge of the rotor disc to the aft part to the tail.

It is assumed that the gust is invariant in the lateral sense as demonstrated in the plan view of the rotor, Figure 8. For calculation purposes, the rotor disc is partitioned into lateral strips of constant wind speed. After each simulation time step the rotor disc advances through the turbulence field and all four blades rotate through the appropriate angle. At each blade radial station the aerodynamic velocities are computed and numerical integration performed in the conventional manner.

Gradual penetration of a gust is found to give considerably different results, as illustrated in Figure 9, to the gust which instantaneously engulfs the entire rotor system.

Referring to Figure 9, the 5 m/s instantaneous horizontal gust produces a response similar to that predicted by the simple derivative model, namely positive pitch and roll rates. However, the results for the same individual blade model, but with gradual penetration of the gust field, show a much slower build-up in roll rate and an initial sign

reversal in pitch rate. In contrast, the instantaneous model for a vertical gust predicts a relatively lower aircraft response than with the gust field.

In Figure 10, the comparison is made between the individual blade model with gust penetration and the quasi-stationary model with instantaneous gusts. The example given, this time, is for a stochastic disturbance at an aircraft speed of 100 km/hr.

Typical computation times (CPU), as run on an IBM 370/168, ranged from 11 sec., for a simple derivative model, to 137 sec. for the individual blade model (in both instances for a 10 sec. simulation time). In cases where a large step gust was employed, computation times for the quasi-stationary model were found to exceed those of the individual blade model owing to the longer time required to trim the rotor.

2.4 Pilot Model

It is quite often convenient to obtain gust response information from a simulation assuming no pilot intervention, the classical "controls fixed" calculation. This is particularly so when using one of the discrete gust disturbances to compare various rotor systems or calculate extreme loading conditions. However, for a simulation lasting more than a few seconds, the assumption of controls fixed becomes less realistic, especially when investigating the least stable sections of the flight regime. It must be assumed that, without automatic stabilization equipment engaged, the pilot is likely to react to disturbances after approximately 2-3 seconds, in order to prevent unpleasant or dangerous aircraft motions developing.

For these reasons, an aircraft pilot model is introduced to investigate the longer term helicopter performance. It is recognized that it is not possible to model all aspects of a pilot since his reactions will vary owing to many conditions such as environment, work load, fatigue and training. In fact, a well trained pilot is able to adapt to the conditions and equipment in order to produce a satisfactory output. The pilot model must therefore be chosen to represent his minimum possible achievement rather than his optimum performance. Reference [6], from which the following model has been extracted, contains a good explanation of pilot behaviour (Figure 11).

$$Y_P(s) = K_P \cdot e^{-s \cdot \tau} \cdot \frac{1 + T_L \cdot s}{1 + T_N \cdot s} \quad (6)$$

where $e^{-s \cdot \tau}$ is a pure time delay $\tau = 0,2$ sec.

$\frac{1}{1 + T_N \cdot s}$ is a neuromuscular delay $T_N = 0,1$ sec.

K_P is the pilot's gain and a function of the task
 $1 + T_L \cdot s$ is any lead compensation that the pilot is able to perform in order to improve the output error.

In section 3 results are presented for a number of helicopter case studies. For this work pilot models were used in the pitch, roll, and yaw loops, the parameters being adjusted with the aim of producing optimal damping ($\zeta = 0,7$) within achievable values. In the special case of hover, a more complex cross-coupled model was devised with feedback variables including velocities and distances, as well as pitch and roll angles, in an attempt to produce a more realistic simulation of the pilot maintaining the aircraft's position with respect to the ground.

3. Simulation Examples

In this section, some simulation examples are presented showing the effect of blade flapping stiffness and flight speed on the piloting task. The leading particulars of the configurations investigated are listed in Table 1. The data for case helicopter I, with an equivalent flapping hinge offset of 14%, is typical of the MBB BO 105. Helicopter II has a 2% hinge offset, a value common for fully articulated rotor systems. Helicopter III with the 0% hinge offset represents the teetering rotor system. No attempt was made to optimize the three configurations, so that the only difference between them was the flapping stiffness.

The eigen values for the unstabilized aircraft in the longitudinal plane are shown in Figure 12. It can be seen that at 100 km/hr both the 2% and 0% hinged rotors are on the border line of stability, with the 14% rotor slightly unstable. However, referring to the controllability diagram (Figure 12) the 0% rotor emerges as a marginally acceptable design, the 2% acceptable and the 14% lies well within the controllability specification.

In all cases presented in this section, the results were calculated using the individual blade model combined with a 2-dimensional stochastic gust field. The wind parameters were set for a mean speed of $U_m = 7$ m/s with turbulence intensities $\sigma_u = 1,5$ m/s and $\sigma_w = 1,4$ m/s. In each case, a pilot model was included so as to stabilize the helicopter with good damping qualities, as discussed in section 2.4.

The time histories for selected variables of helicopter I (14% hinge), at a trimmed flight speed of 100 km/hr are shown in Figure 13. It can be seen that there is a reasonable amount of pilot control activity in both longitudinal (D_β) and lateral (D_α) cyclic, with a tendency for greater angular velocities in roll rather than pitch, owing to the cross-couplings associated with rotors of this stiffness. By comparison with the results for helicopter II (2% hinge), shown in Figure 14, it can be seen that the "softer" rotor has a weaker pitch and roll cross-couplings, as is indicated by the pilot lateral control activities.

The time histories for helicopter III (0% hinge) give a rather over-pessimistic view of the teetering rotor performance. This is partially due to low damping and control powers of configuration III, as shown in Figure 12, and partially due to the type of pilot model used in the simulation.

For example, in flying a teetering rotor helicopter, the pilot will often compensate for the slowness in pitch response by sensing other parameters, such as observing changes in the rotor tip-path-plane, and making corresponding corrective action.

For a more quantitative assessment of piloting ability, it is usual to evaluate a performance index, relating to the deviation away from the desired course. For example, criteria that can be used are the standard deviation away from the mean or the integral squared error which includes a time weighting factor,

$$A_q = \int_0^{\infty} (x_i - \bar{x})^2 \cdot dt \quad (7)$$

The standard deviations and integral squared errors have been calculated for the three case studies above and are presented in Table 2. It can be seen that in nearly all cases the 14% hinged rotor system returns the lowest standard deviations, indicating more accurate flight path control with smaller control amplitudes. The pitch-roll cross-coupling is evident in configuration I (14%) by the larger index for lateral cyclic (η_y) over that for longitudinal (η_x) while helicopter II (2%) has less pitch-roll cross-coupling as previously discussed.

Finally, the influence of forward speed on the standard deviations is shown in Figure 16. Standard deviations away from the flight path (σ_θ , σ_ϕ) vary little with speed but the control variables (σ_{η_x} , σ_{η_y}) reflect the velocity dependent pitch-roll cross-coupling.

This coupling is particularly strong in hover and at low speed, as can be seen from the comparable values for σ_{η_x} and σ_{η_y} . With an increase in flight speed, the downwash field changes, and the coupling becomes less pronounced so that at high speed the pilot's work load is predominantly in the longitudinal control sense η_x . The increasing standard deviation of load factor (σ_n), as speed increases, derives from the greater vertical gust sensitivity at the higher speed.

Conclusions

The discrete gust model is adequate for use in the understanding of rotor behaviour. However, the stochastic model and the validity of the frozen field concept must come under question when applied to helicopters at hover and low forward speeds, in which states the rotor wake is likely to have a direct influence.

Progressive gust penetration by the rotor is an important feature which should be included, where possible, as it is likely to strongly influence the simulation results. Consequently, the individual blade model with the gust field model should be used when high computation time is permissible.

Despite the reduction in high speed forward flight stability normally associated with it, a rotor system of the semi-hingeless type (14% equivalent flapping hinge offset) will usually have a better gust performance (low pilot control inputs, less deviation from course) than a conventional articulated rotor (2% equivalent flapping hinge offset).

References

- 1) -, Military Specification Flying Qualities of Piloted Aeroplanes, MIL-F-8785B (ASG), 1969/1971
- 2) -, Wind Model for Landing Simulations. United Kingdom Air Registration Board, ARB 417
- 3) O.H. Gerlach, G. van de Moesdijk, and J.C. van der Vaart, Progress in the Mathematical Modelling of Flight in Turbulence, AGARD Conference Proceedings No. 140 on Flight in Turbulence, Paper No. 5, May 1973
- 4) G. Schänzer, Böenmodelle für Anwendungen in der Flugdynamik, Zeitschrift Flugwiss. Weltraumforsch. 1 (1977) Heft 3
- 5) G. van de Moesdijk, Non-Gaussian Structure of the Simulated Turbulent Environment in Piloted Flight Simulation, Delft University of Technology Netherlands, M-304, April 1978
- 6) D.T. Mc Ruer, E.S. Krendel, Mathematical Models of Human Pilot Behaviour, AGARDograph No. 188, January 1974
- 7) -, Aeroplane Strength and Rigidity Reliability Requirements, Repeated Loads and Fatigue, MIL-A-8866 (ASG)
- 8) F.E. Pritchard et al. Spectral and Exceedance Probability Models of Atmospheric Turbulence for Use in Aircraft Design and Operation, AFFDL-TR-65-122, 1965

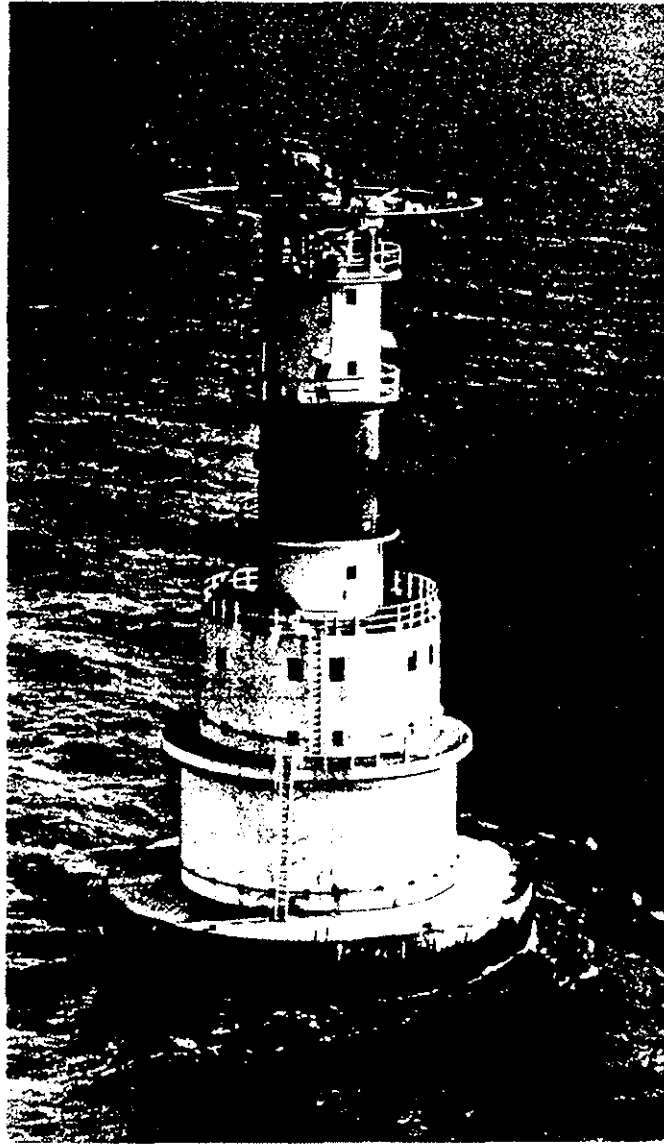


Figure 1: BO 105 AT WORK

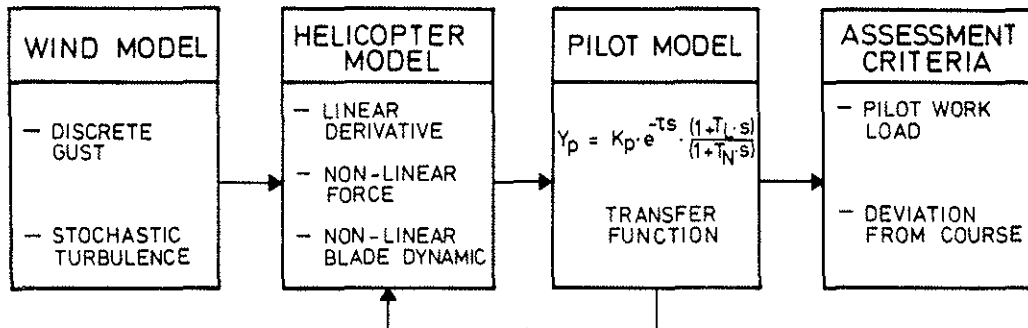


Figure 2: TURBULENCE SIMULATION ELEMENTS

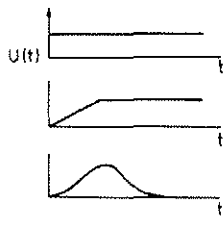
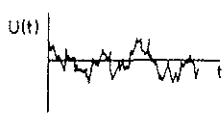
WIND MODEL	FORM	APPLICATION
DISCRETE GUST		FLIGHT LOADS CALCULATION FREQUENCY ANALYSIS DERIVATIVE ESTIMATION
STOCHASTIC TURBULENCE		PILOT WORK LOAD OVERALL ASSESSMENT

Figure 3: WIND MODELS

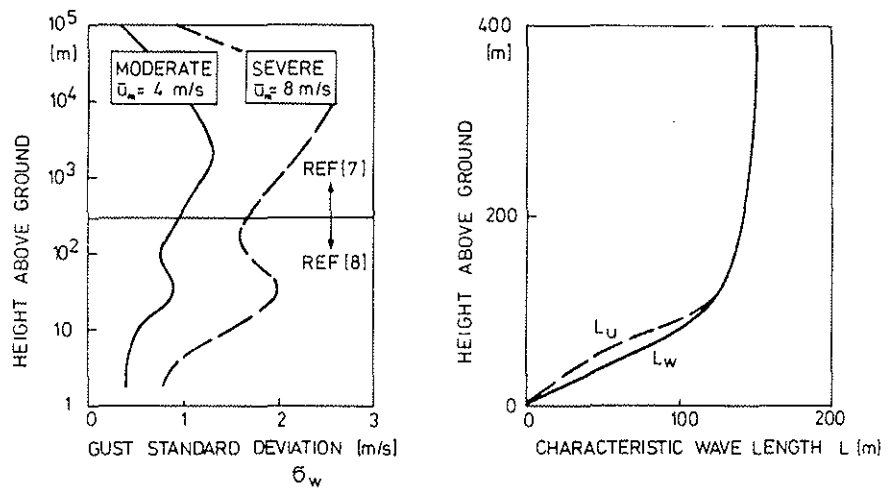


Figure 4: INFLUENCE OF ALTITUDE ON TURBULENCE PARAMETERS

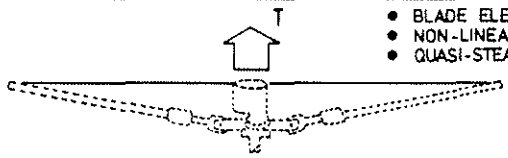
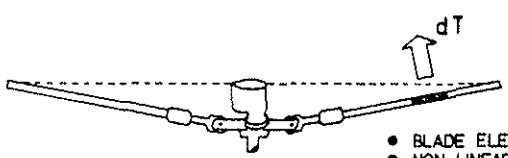
DERIVATIVE	$\dot{\underline{x}} = A \cdot \underline{x} + B \cdot \underline{u}$
QUASI - STATIONARY	 <ul style="list-style-type: none"> • BLADE ELEMENT THEORY • NON-LINEAR AERODYNAMICS • QUASI-STEADY BLADE DYNAM
INDIVIDUAL BLADE	 <ul style="list-style-type: none"> • BLADE ELEMENT THEORY • NON-LINEAR AERODYNAMICS • INDIVIDUAL BLADE TRANSIENT DYNAMICS

Figure 5: HELICOPTER MODELLING METHODS FOR FLIGHT DYNAMIC SIMULATION

Figure 6: HELICOPTER INDIVIDUAL BLADE MODEL

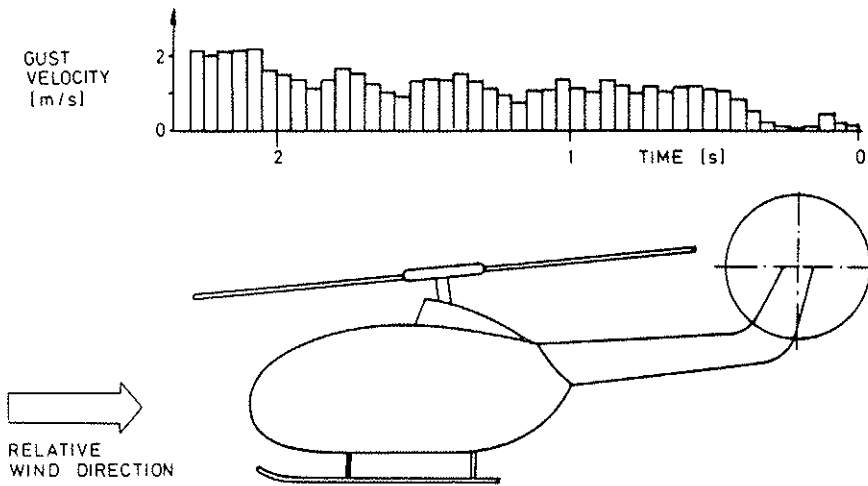
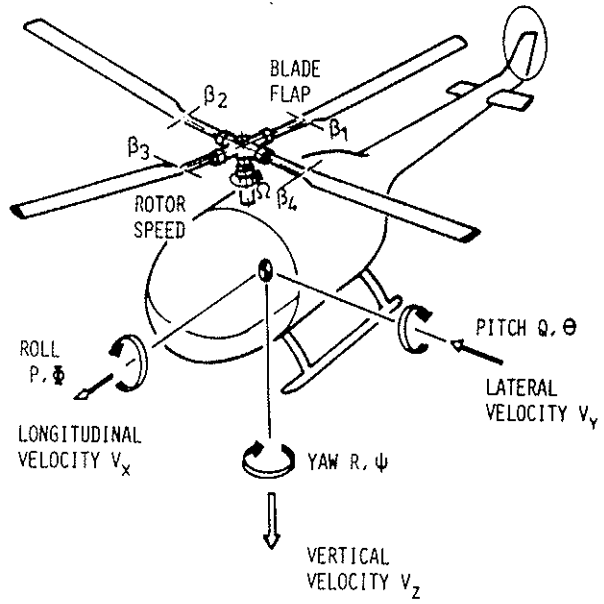


Figure 7: SIMULATION WITH GRADUAL GUST PENETRATION

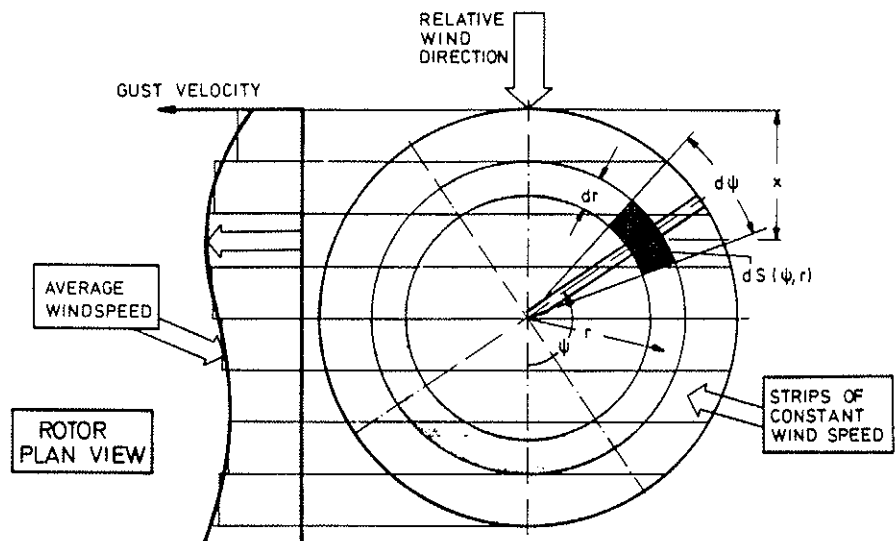


Figure 8: INTERPRETATION OF GUST FIELD OVER THE ROTOR

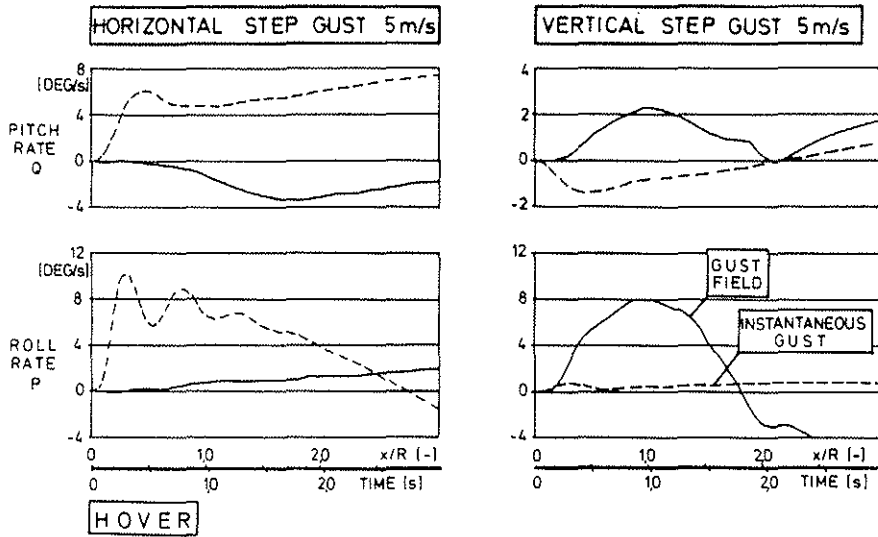


Figure 9: COMPARISON BETWEEN INSTANTANEOUS AND GRADUAL GUST PENETRATION

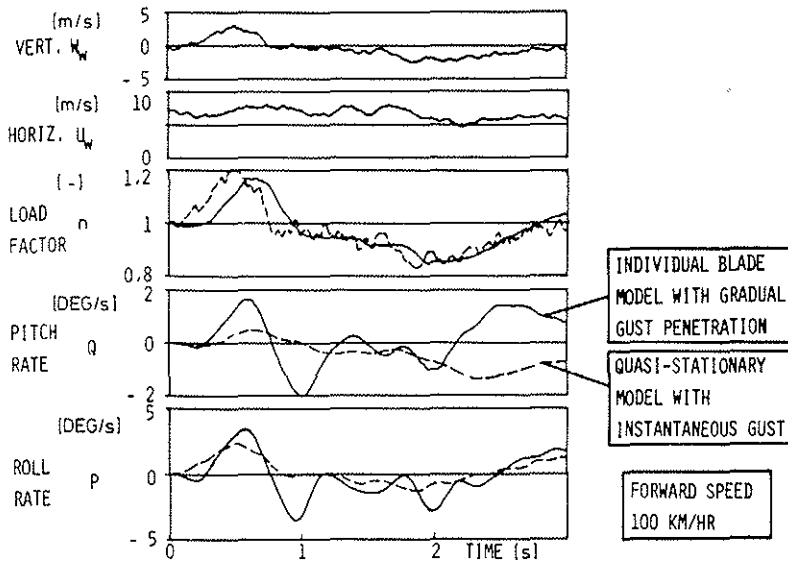


Figure 10: COMPARISON BETWEEN QUASI-STATIONARY AND INDIVIDUAL BLADE MODELS

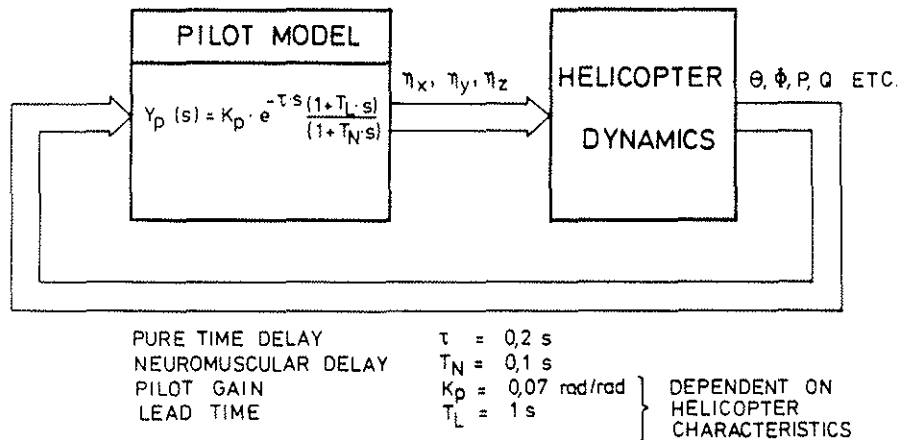


Figure 11: PILOT MODEL

PARAMETER		CASE HELICOPTER		
		I	II	III
MASS	m (kg)		2100	
PITCH INERTIA	I_{yy} (kgm ²)		4000	
ROLL INERTIA	I_{xx} (kgm ²)		1314	
MASS CENTRE (FORWARD FROM ROTOR SHAFT)	x_s (m)		0.08	
ROTOR RADIUS	R (m)		4.912	
BLADE NO.	n (-)		4	
CHORD	c (m)		0.27	
ROTOR ROTATIONAL SPEED	Ω (rad/s)		44.4	
EQUIVALENT HINGE OFFSET (ZERO SPRING)	a_β/R (%)	14	2	0

Table 1: HELICOPTER DATA

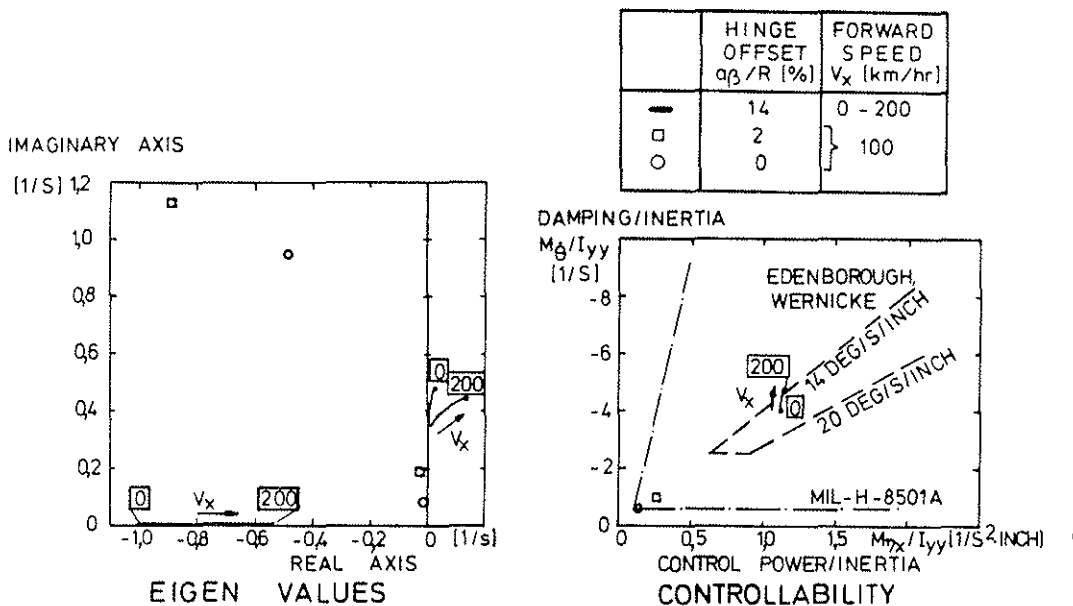


Figure 12: STABILITY AND CONTROL CHARACTERISTICS OF SIMULATION EXAMPLES

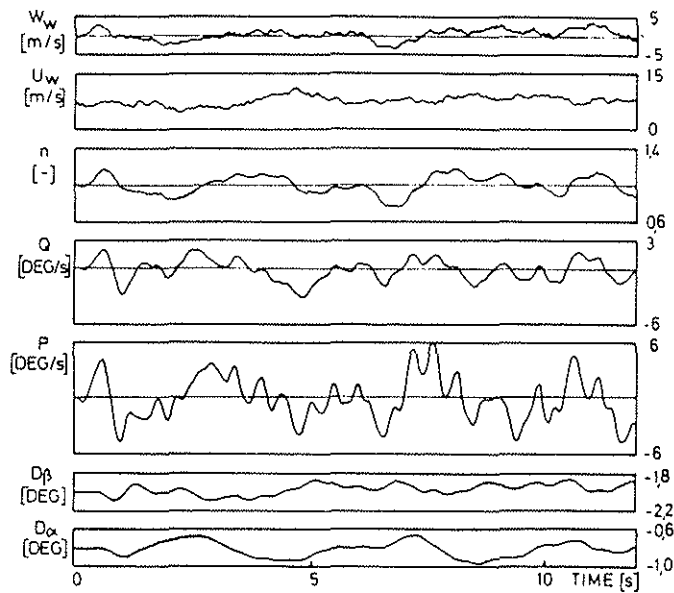


Figure 13:
TURBULENCE SIMULATION WITH PILOT
(14% EQUIV. FLAPPING HINGE OFFSET)

FORWARD SPEED
100 km/hr.

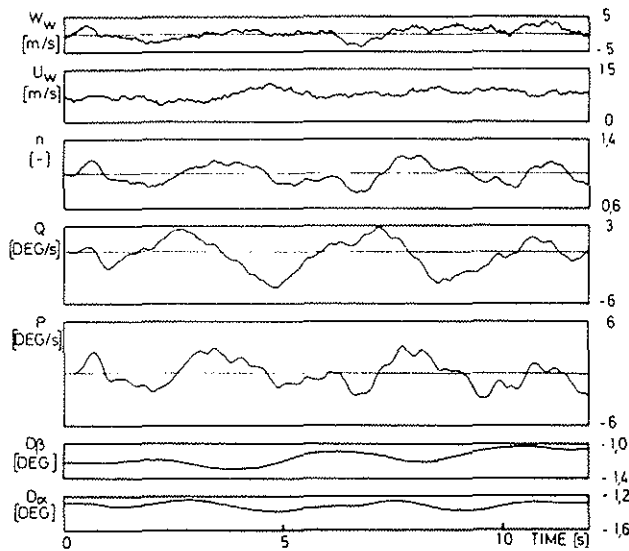


Figure 14:
TURBULENCE SIMULATION WITH PILOT
(2% EQUIV. FLAPPING HINGE OFFSET)

FORWARD SPEED
100 km/hr

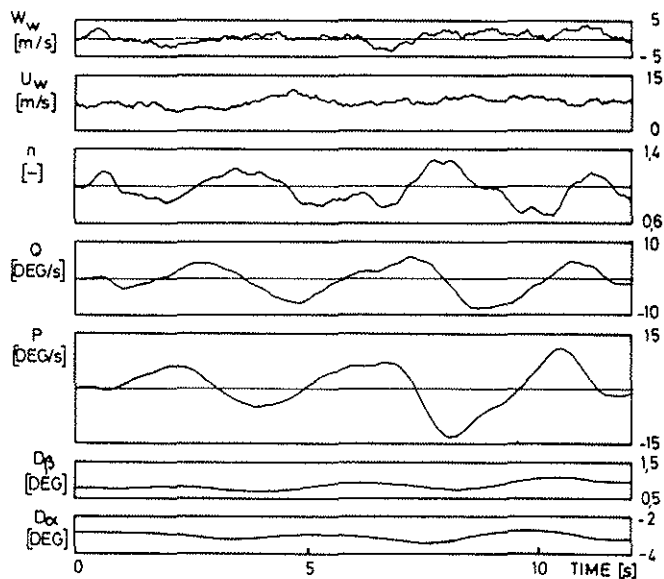


Figure 15:
TURBULENCE SIMULATION WITH PILOT
(0% EQUIV. FLAPPING HINGE OFFSET)

FORWARD SPEED
100 km/hr

HELICOPTER	A B C D E F G H I J K L M N	DEVIATION FROM TRIM						CONTROL ACTIVITY	
		ϕ [DEG]	θ [DEG]	ψ [DEG]	V_x [m/s]	V_z [m/s]	n [-]	n_x [mm]	n_y [mm]
$a_{\beta}/R = 14\%$	σ	0,97	1,26	0,59	0,48	0,63	0,098	1,77	2,06
	peak-to-peak	3,75	3,44	2,01	1,33	2,50	0,41		
	A_q							38,26	46,5
$a_{\beta}/R = 2\%$	σ	1,04	2,37	0,79	0,78	0,79	0,107	2,27	1,03
	peak-to-peak	3,26	6,49	2,13	2,64	2,80	0,43		
	A_q							70,15	13,3
$a_{\beta}/R = 0\%$	σ	5,82	5,06	5,74	1,44	2,04	0,15	3,54	6,19
	peak-to-peak	16,75	13,34	9,53	4,47	4,90	0,74		
	A_q							140,3	445,1

Table 2: PERFORMANCE COMPARISON OF HELICOPTER CASE STUDIES

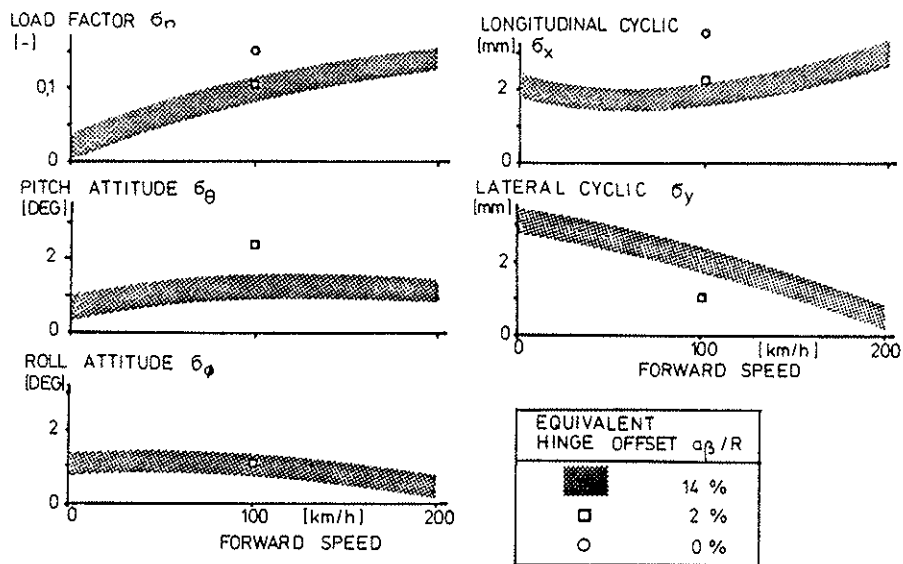


Figure 16: VARIATION OF STANDARD DEVIATIONS σ WITH FORWARD SPEED